CANOPY NITROGEN ESTIMATION ON COTTON PLANT USING SATELLITE IMAGERY

B. J. Chew[1] *, W. Wiratama[1], M. H. Goh[1]
[1] ST Engineering Geo-Insights Pte Ltd, Singapore – (chew.boonjin, wahyu.wiratama, minhua.goh)@stengg.com

KEY WORDS: Canopy nitrogen prediction, satellite imagery, remote sensing, Sentinel 2, vegetation indices.

ABSTRACT:

The optimization of nitrogen (N) management is becoming a key challenge to enhance crop yield production while protecting the environment. Analysis of canopy N content in crop plants is used as insights for fertilization management, in which actions can be taken to optimize N fertilizer usage. Traditionally, lab chemical processing is used to measure the crop plant's nutrient content. However, the collection of leaf samples from the field is labour intensive, and it would be costly to increase sampling frequency. Thus, this approach may not be the most optimal for large plantations. Remote sensing applications in agriculture have been widely studied. This study aims to evaluate the potential of using Sentinel 2 imagery to predict canopy N content, as an alternative wide scale method as compared to traditional methods. A cotton plantation with about 50 square km area in the state of Mato Grosso, Brazil, was used as the case study. About 180 samples across the cotton plantation were collected between March and April 2022 and the N contents of the crop plants were measured using lab chemical processes. Sentinel 2 images within 15 days of the sampling dates were retrieved from ESA's Copernicus Open Access Hub. This study proposes a Random Forest (RF) regression algorithm for the generation of an N prediction model. About 52 vegetation indices (VIs) were extracted as the features for model training, such as Normalized Difference Vegetation Index (NDVI) and Enhanced Vegetation Index (EVI). RF model allows easy measurement of the relative importance of each feature with respect to the prediction to achieve a good performance. Validation is done by using mean absolute error (MAE) and mean absolute percentage error (MAPE) to evaluate the prediction accuracy against the ground truth, which resulted to be 3.418 g/kg and 9.29% respectively. Finally, this study analyses the performance of the canopy N prediction model and assesses its ability as an alternative to traditional lab chemical sampling processes.

1. INTRODUCTION

Increasing global demand for agricultural products have resulted in more intensive farming that causes drains nutrients from the soil (Purwanto & Alam, 2019). Application of fertilizer replaces the nutrients for crop uptake which otherwise would have been insufficient. However, over-fertilisation of crop land occurs worldwide and may cause environmental issues due to surface run-off into the natural environment (Ritchie, 2021; Sishodia et al., 2020). Furthermore, application of excess fertiliser contributes to additional costs. This pushes for a need to identify the optimal amount of fertiliser to minimise cost as well as maintaining yield. This optimal amount depends on the plant status and thus the requirement to have an accurate estimate of the plant nutrient status.

Nitrogen is an important element in the plant, and is present in chlorophyll, amino acids and hence protein, nucleic acids, plant tissue, etc (Buchholz, 2022). Traditionally, N level can be obtained via lab chemical processing, however, this process takes time and increases the operational costs (Farella et al., 2022). Furthermore, the sampling results only applies for that set of leaf samples and does not represent the entire crop field. There is a need to consider alternate methods of estimating leaf nutrient that is cheaper and faster.

Satellite-based remote sensing provides an advantage in wide area monitoring and have been used for many different applications in agriculture, such as land use and crop classification, soil health and moisture, and vegetation health (Sishodia et al., 2020). Satellites such as European Space Agency's Sentinel 2 provides global coverage over land once every 5 days and have a wide imaging swath of 290 km (Sentinel-2). Sentinel 2 L2A product has 12 bands ranging from visible to short wave infrared at spectral resolutions ranging from 10m to 60m. It is provided for public access and is atmospherically corrected, hence it is a surface reflectance product. Band combinations – such as band ratios, normalised band differences, or more complex formulae – can be derived for different purposes. There are many indices derived for agricultural purposes, such as Normalised Difference Vegetation Index (NDVI) and Enhanced Vegetation Index (EVI). These vegetation indices (VI) have their own advantages and limitations. One example is the usefulness of NDVI to determine broadly the vigour of a vegetated area, however it faces an oversaturation issue where NDVI value loses sensitivity beyond a vegetation density (Pettorelli et al., 2005).

Machine learning can be used to estimate nitrogen levels on crop leaves using satellite imagery by collecting data, extracting relevant features, training a machine learning model, and validating the model. Marang et al. (2021) proposed hybrid random forest regression, DBSCAN, and PCA to predict N level on cotton crop using hyperspectral UAV and sentinel imagery. Huang et al. (2015) estimated rice nitrogen status based on satellite imagery. R-squared was used to compute relationship between vegetation indices and rice N status. Moreover, Tan et al. (2020) proposed partial least square and remote sensing imagery to predict protein content.

Random forest (RF) regression is one of the common machine learning methods which have been used in estimation of foliar nitrogen levels (Abdel-Rahman et al., 2012; Soltanikazemi et al., 2022). RF is an ensemble method which uses a decision tree as a base estimator. It allows for easy measurement of the relative importance of each feature with respect to the prediction, hence achieving a good performance. In this study, we attempted to use RF regression model to estimate foliar nitrogen concentrations for cotton crops in Brazil. We want to validate the performance

https://doi.org/10.5194/isprs-archives-XLVIII-M-1-2023-73-2023

of applying RF regression model on selected indices based on Sentinel 2 and determine the limitations of the model.

2. STUDY AREA AND DATA COLLECTION

In this paper, field experiments were conducted from February to April 2022 over a cotton plantation in the state of Mato Grosso, Brazil with about 50 square km area, as shown in Figure 1. Leaf samples were collected during the vegetative and flowering stage of the cotton plants, between 70 to 120 days after emergence. The sampling process involve by first identifying a sampling coordinate (latitude, longitude) within the plantation. Leaf samples are then collected randomly within a 10m radius from the sampling coordinate. This process was iterated across different sampling coordinates and dates. Afterwards, the samples were handled by a professional vendor to measure the nitrogen content using chemical laboratory equipment, carried out with standardized procedure. The measured leaf nitrogen concentration of the leaf samples was then provided as g/kg. In this study, 180 samples were collected and used to generate and validate our model. The statistics of the sampled nitrogen concentration is as shown in Table 1 below.

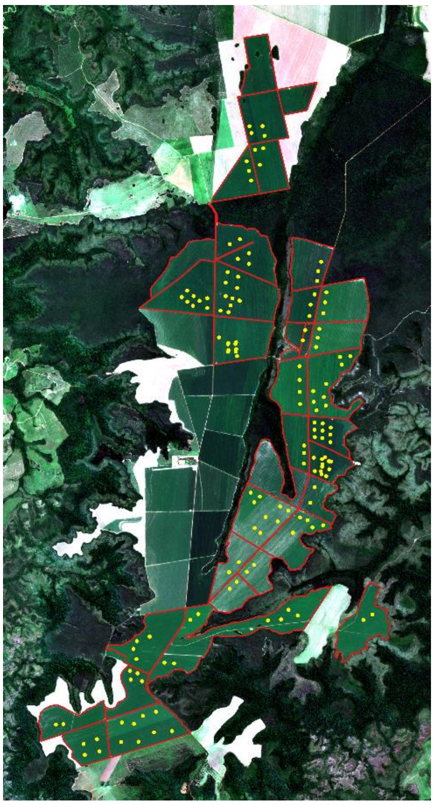

Figure 1. Cotton Plantation Area

Mean	Standard Deviation	Min	Max
38.3	5.15	23.5	52.6

Table 1. Statistics of Nitrogen samples in g/kg

We collected cloud-free Sentinel-2 L2A data that fall within 15 days from the sample date for each sampling coordinate. L2A products were used for our processing as the atmospheric effects were removed. We then up-sampled all bands to 10m spatial resolution, before extracting the 3x3 context pixels centred on the sampling coordinates. Vegetation indices (VIs) were computed to obtain the percentage of vegetation cover, amount of chlorophyll content, leaf area, and so on (As-Syakur et al. 2012; Brecht 2018; Broge and Leblanc 2001; Chen 1996; Duong et al. 2017; El-Shikha et al. 2008; Frampton et al. 2013; Gitelson et al. 2002; Hiphen-plant 2022; Huang et al. 2012; Main et al. 2011; Metternicht 2003; NDRE index 2023; Pro.arcgis; Rasul et al. 2018; Sentinel Hub; Vincini et al. 2008; Waqar et al. 2012; Xu 2006; Zhao and Chen, 2005). A total of 52 VIs were computed to get handcrafted features, as described in the Appendix. After which, 52 VIs and 12 bands were deployed as the feature inputs to the RF model.

3. METHOD

Figure 2 shows the overall flowchart of the proposed method, including pixel extraction, feature extraction, and RF regression model. Firstly, Sentinel-2 images and sample coordinates were used to retrieve sampled foliar nitrogen values and their respective pixels. The 52 VIs were then computed. Next, the training dataset was generated from the 12 bands and 52 VIs. The best hyperparameters of the RF model were chosen with reference to the training dataset, with the aid of Random Search CV optimization algorithm. Table 2 shows the hyperparameters that were fed into the optimization algorithm. The dataset was then incorporated into the model for training.

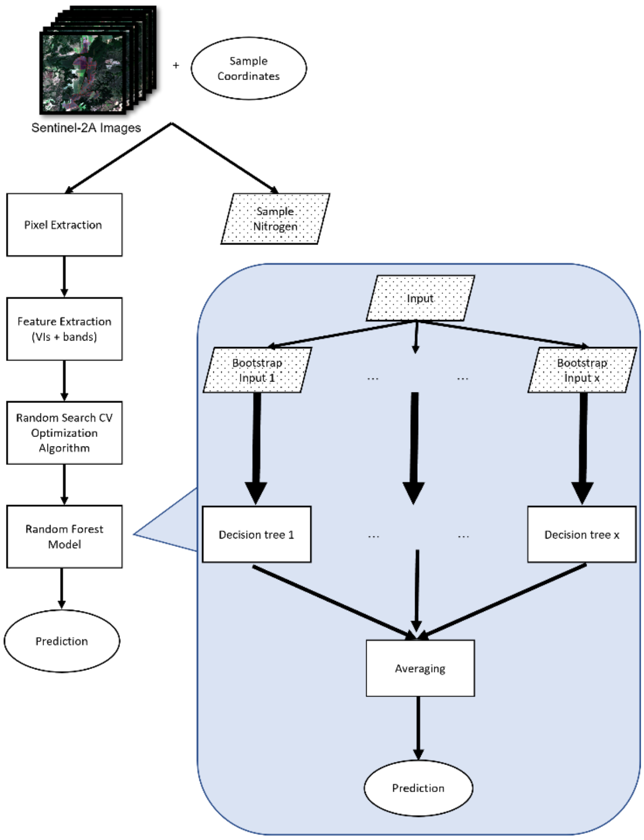

Figure 2. Overall Flowchart

https://doi.org/10.5194/isprs-archives-XLVIII-M-1-2023-73-2023 | © Author(s) 2023. CC BY 4.0 License.

Parameters	Hyperparameters values
Max depth	[10, 20, 30, 40, 50, 60, 70, 80, 90, 100]
Max features	[‘auto’, ‘’sqrt]
Min sample leaf	[1, 2, 4]
Min sample split	[2, 5, 10]
N estimators	[200, 400, 600, 800, 1000, 1200, 1400, 1600, 1800, 2000]

Table 2. Settings for Hyperparameter Values as Input to the Random Search CV Algorithm

4. PERFORMANCE EVALUATION

Figure 3 shows the histogram of the dataset where we observe most N values ranged between 33 and 47 g/kg, therefore we assumed that values beyond this range were extreme values. In the experiment, we split the dataset randomly into 80% training and 20% testing with respect to the observed value.

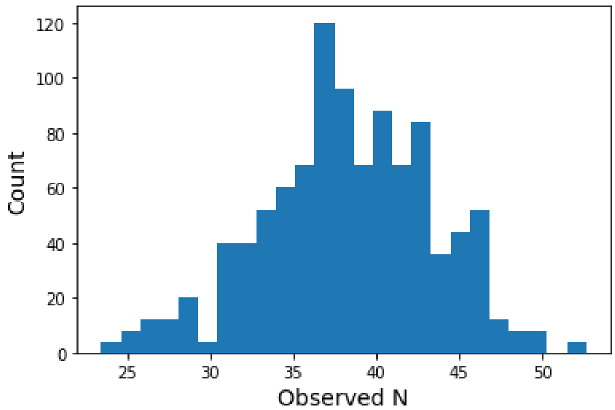

Figure 3. Histogram of Dataset

The optimized RF model was trained using the training dataset, generating the feature importance scores as shown in Figure 4 below. It was shown that the top 15 features were the most important on the N prediction, namely Band 11, Band 1, IRECI, Band 5, MNDWI, BRBA, CCCI_ALT, Band 12, Band 9, NDVI3, MCARI_ALT, BUI, Band 2, Band 3, and NPCI.

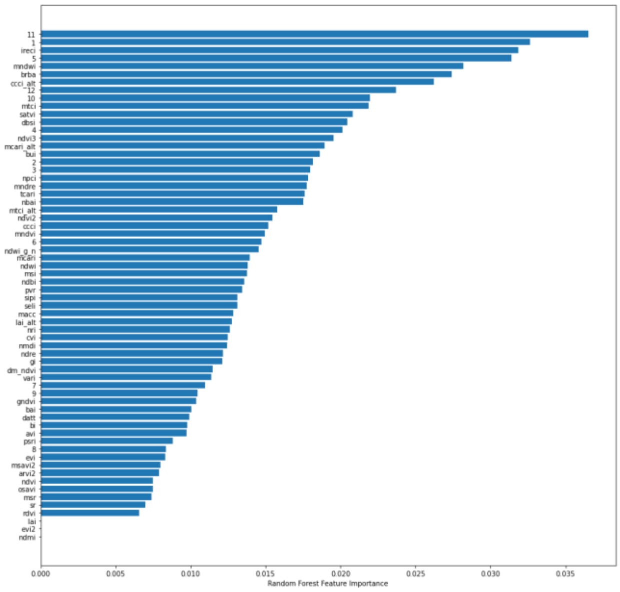

Figure 4. Random Forest Feature Importance

The model was further evaluated using the mean absolute error (MAE) and mean absolute percentage error (MAPE). MAE is a common metric used to evaluate the performance of prediction model by measuring the average absolute difference between the observed and predicted values. MAPE is similar to MAE, except the average absolute difference is being divided by the observed value before summation. The formulas of MAE and MAPE are as shown below:

$$MAE = \frac{1}{n}\sum_{i=1}^{n}\left|y_{actual} - y_{predicted}\right| \quad (1)$$

$$MAPE = \frac{100}{n}\sum_{i=1}^{n}\frac{\left|y_{actual} - y_{predicted}\right|}{y_{predicted}} \quad (2)$$

where n = number of samples
y_{actual} = observed value
$y_{predicted}$ = predicted value

Figure 5 below depicts the prediction plot using training and testing data that gives a fit prediction for training data. According to our experiment, this study presents MAE of 3.418 g/kg, which is MAPE of 9.29% for the testing dataset.

We observe that the model is able to achieve a better performance for N prediction where the values fall within the middle range highlighted above. Poorer performance for the extreme values could be attributed to lack of training data in that range, and that training with an imbalanced dataset resulted in higher errors. In addition, it is believed that the model loses sensitivity at the extreme ends of the distribution and the dataset is still lacking features with high correlation to N. Increase in variance of N distribution and the size of the dataset can be an alternative solution in the future to overcome the overfitting issue. Moreover, hyperspectral (HS) images can be an option to increase the number of features available for training since they are more sensitive than S2A images, which are multispectral images.

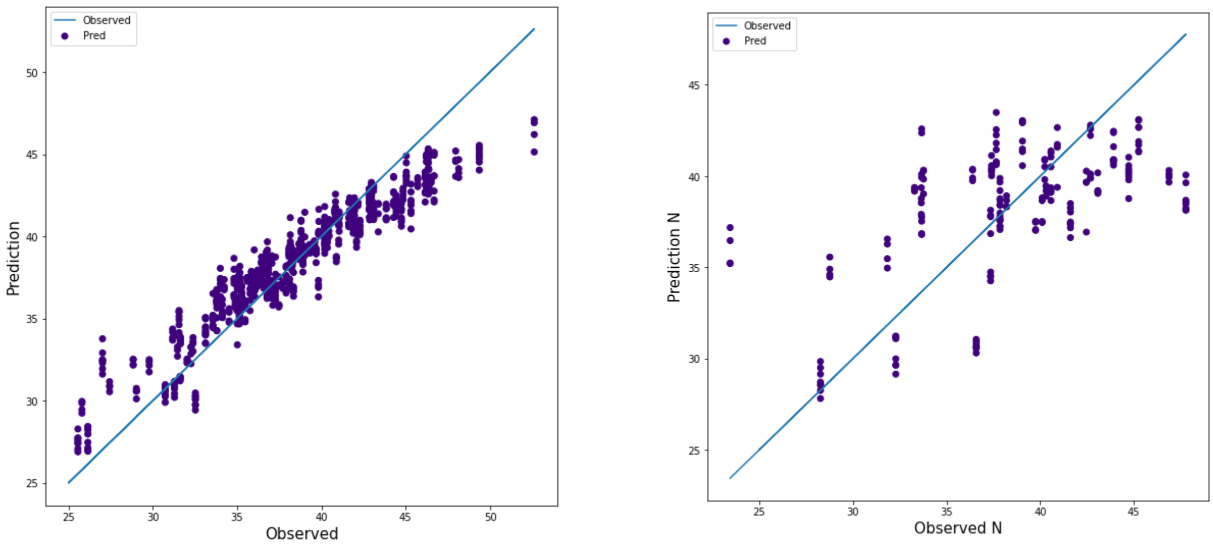

a). Prediction Plot using Training Data

b). Prediction Plot using Testing Data

Figure 5. Prediction Plot a). using Training Data, b). using Testing Data

5. CONCLUSION

This study proposed the use of Sentinel-2 imagery and machine learning method, specifically RF model, to predict the amount of N present in the canopy of the cotton crops, in hopes of replacing the traditional method, with the end goal to save cost and time. RF model was chosen since it could calculate which feature was important to the prediction to achieve a high accuracy, with the top 15 features being the most important on the N prediction to be Band 11, CSI, Band 1, IRECI, Band 5, MNDWI, BRBA, CCCI_ALT, Band 12, Band 9, NDVI3, MCARI_ALT, BUI, Band 2, Band 3. The validation metric used was MAE which resulted to be 3.418 g/kg, which was MAPE of 9.29% for the testing dataset. While MAE is considerably low, more could be done since MAE was mostly contributed by the inaccurate prediction of extreme N values. Improvements such as using hyperspectral imagery instead of Sentinel-2 imagery and using different VIs of different feature importance based on different methods could be done. Even though VIs among different methods could be of different feature importance, stacking them with the consideration of different methods could prevent overfitting and should be used to monitor agricultural fields to improve classification accuracy. In addition, boosting the dataset with more data, especially in the extreme range, would help to resolve the imbalanced dataset issue.

REFERENCES

Abdel-Rahman, E. M., Ahmed, F. B., Ismail, R. (2012). Random Forest regression and spectral band selection for estimating sugarcane leaf nitrogen concentration using EO-1 hyperion Hyperspectral Data. International Journal of Remote Sensing, 34(2), 712–728. https://doi.org/10.1080/01431161.2012.713142

As-Syakur, A.R., Adnyana, I.W.S., Arthana, I.W. and Nuarsa, I.W., 2012. Enhanced built-up and bareness index (EBBI) for mapping built-up and bare land in an urban area. Remote sensing, 4(10), pp.2957-2970. doi.org/10.3390/rs4102957

Brecht, 2018, Remote sensing indices, https://medium.com/regen-network/remote-sensing-indices-389153e3d947, accessed by 19 January 2023.

Broge, N.H., Leblanc, E., 2001, Comparing prediction power and stability of broadband and hyperspectral vegetation indices for estimation of green leaf area index and canopy chlorophyll density. Remote Sensing of Environment. 76. 2. 156-172. doi.org/10.1016/S0034-4257(00)00197-8

Buchholz, D. 2022, March. Nitrogen in the plant. University of Missouri Extension. https://extension.missouri.edu/publications/wq259, accessed by 20 January 2023.

Chen, J.M., 1996. Evaluation of vegetation indices and a modified simple ratio for boreal applications. Canadian Journal of Remote Sensing, 22(3), pp.229-242. doi.org/10.1080/07038992.1996.10855178

Duong, T., Chou, T., Fang, Y., 2017. Integration of GIS and Remote Sensing for Evaluating Forest Canopy Density Index in Thai Nguyen Province, Vietnam. International Journal of Environmental Science and Development. 8. 539-542. doi.org/10.18178/ijesd.2017.8.8.1012.

El-Shikha, D. M, Barnes, E. M, Clarke, T. R, Hunsaker, D. J, Haberland, J. A, Pinter, P. J, Waller, P. M, & Thompson, T. L., 2008. Remote Sensing of Cotton Nitrogen Status Using the Canopy Chlorophyll Content Index (CCCI). Transactions of the ASABE, 51, 73-82. doi.org/10.13031/2013.24228

Farella, M. M., Barnes, M. L., Breshears, D. D., Mitchell, J., van Leeuwen, W. J., & Gallery, R. E., 2022. Evaluation of vegetation indices and imaging spectroscopy to estimate foliar nitrogen across disparate biomes. Ecosphere, 13(3). https://doi.org/10.1002/ecs2.3992

Frampton, W., Dash, J., Watmough, R.G., Milton, E.J., 2013. Evaluating the capabilities of Sentinel-2 for quantitative estimation of biophysical variables in vegetation. ISPRS Journal of Photogrammetry and Remote Sensing. 82. 83–92. doi.org/10.1016/j.isprsjprs.2013.04.007.

Gitelson, A., Kaufman, Y., Stark, R., Rundquist, D., 2002. Novel Algorithms for Remote Estimation of Vegetation Fraction. Remote Sensing of Environment. 80. 76-87. doi.org/10.1016/S0034-4257(01)00289-9.

Hiphen-plant, 2022, Vegetation Indices for Chlorophyll, www.hiphen-plant.com, accessed by 20 January 2023.

Huang, W., Luo, J., Zhang, J., Zhao, J., Zhao, C., Wang, J., Yang, G., Huang, M., Huang, L. and Du, S., 2012. Crop disease and pest monitoring by remote sensing. In Remote Sensing-Applications. IntechOpen. doi.org/10.5772/35204

Huang, S., Miao, Y., Zhao, G., Yuan, F., Ma, X., Tan, C., Yu, W., Gnyp, M.L., Lenz-Wiedemann, V.I., Rascher, U. and Bareth, G., 2015. Satellite remote sensing-based in-season diagnosis of rice nitrogen status in Northeast China. Remote sensing, 7(8), pp.10646-10667. doi.org/10.3390/rs70810646

Main, R., Cho, M.A., Mathieu, R., O’Kennedy, M.M., Ramoelo, A., Koch, S., 2011. An investigation into robust spectral indices for leaf chlorophyll estimation. ISPRS Journal of Photogrammetry and Remote Sensing. 66. 751-761. doi.org/10.1016/j.isprsjprs.2011.08.001

Marang, I.J., Filippi, P., Weaver, T.B., Evans, B.J., Whelan, B.M., Bishop, T.F., Murad, M.O., Al-Shammari, D. and Roth, G., 2021. Machine learning optimised hyperspectral remote sensing retrieves cotton nitrogen status. Remote Sensing, 13(8), p.1428. doi.org/10.3390/rs13081428

Metternicht, G., 2003. Vegetation indices derived from high-resolution airborne videography for precision crop management. Int. J. Remote Sens. 24. doi.org/10.1080/01431160210163074.

NDRE index: Vegetation Analysis in mid and late season. EOS Data Analytics., 2023. https://eos.com/industries/agriculture/ndre/

Pettorelli, N., Vik, J. O., Mysterud, A., Gaillard, J.-M., Tucker, C. J., & Stenseth, N. C., 2005. Using the satellite-derived NDVI to assess ecological responses to environmental change. Trends in Ecology, Evolution, 20(9), 503–510. https://doi.org/10.1016/j.tree.2005.05.011

Pro.arcgis, Indices gallery, https://pro.arcgis.com/en/pro-app/help/data/imagery/indices-gallery.htm, accessed by 20 January 2023.

Purwanto, B. H., & Alam, S., 2019. Impact of intensive agricultural management on carbon and nitrogen dynamics in the Humid Tropics. Soil Science and Plant Nutrition, 66(1), 50–59. https://doi.org/10.1080/00380768.2019.1705182

Rasul, A., Balzter, H., Ibrahim, G.R.F., Hameed, H.M., Wheeler, J., Adamu, B., Ibrahim, S.A. and Najmaddin, P.M., 2018. Applying built-up and bare-soil indices from Landsat 8 to cities in dry climates. Land, 7(3), p.81. doi.org/10.3390/land7030081

Ritchie, H., 2021. Excess fertilizer use: Which countries cause environmental damage by overapplying fertilizers? Our World in Data. Retrieved February 24, 2023, from https://ourworldindata.org/excess-fertilizer

Sentinel Hub, Collection of custom script, https://custom-scripts.sentinel-hub.com/, accessed by 20 January 2023.

Sentinel-2, ESA, https://www.esa.int/Applications/Observing_the_Earth/Copernicus/Sentinel-2, accessed by 21 January 2023

Sishodia, R. P., Ray, R. L., & Singh, S. K., 2020. Applications of remote sensing in Precision Agriculture: A Review. Remote Sensing, 12(19), 3136. https://doi.org/10.3390/rs12193136

Soltanikazemi, M., Minaei, S., Shafizadeh-Moghadam, H., & Mahdavian, A., 2022. Field-scale estimation of sugarcane leaf nitrogen content using vegetation indices and spectral bands of sentinel-2: Application of random forest and support vector regression. Computers and Electronics in Agriculture, 200, 107130. https://doi.org/10.1016/j.compag.2022.107130

Tan, C., Zhou, X., Zhang, P., Wang, Z., Wang, D., Guo, W. and Yun, F., 2020. Predicting grain protein content of field-grown winter wheat with satellite images and partial least square algorithm. PLoS One, 15(3), p.e0228500. doi.org/10.1371/journal.pone.0228500

Vincini, M., Frazzi E., D’Alessio, P., 2008: A broad-band leaf chlorophyll vegetation index at the canopy scale. Precision Agriculture, 9, 303-319. doi.org/10.1007/s11119-008-9075-z

Waqar, M.M., Mirza, J.F., Mumtaz, R. and Hussain, E., 2012. Development of new indices for extraction of built-up area & bare soil from landsat data. Open Access Sci. Rep, 1(1), p.4.

Xu, H., 2006. Modification of Normalized Difference Water Index (NDWI) to Enhance Open Water Features in Remotely Sensed Imagery. International Journal of Remote Sensing. 27. 3025–3033. doi.org/10.1080/01431160600589179.

Zhao, H. and Chen, X., 2005, July. Use of normalized difference bareness index in quickly mapping bare areas from TM/ETM+. In International geoscience and remote sensing symposium (Vol. 3, p. 1666). doi.org/ 10.1109/IGARSS.2005.1526319

APPENDIX

Sentinel-2 L2A bands	Description	Notations
Band 1	Coastal or Aerosol	Co
Band 2	Blue	B
Band 3	Green	G
Band 4	Red	R
Band 5	Vegetation red edge	RE1
Band 6	Vegetation red edge	RE2
Band 7	Vegetation red edge	RE3
Band 8	Near Infrared	NIR
Band 9	Narrow NIR	NNIR
Band 10	Water vapour	WV
Band 11	SWIR	S1
Band 12	SWIR	S2

Table 3. Sentinel-2 L2A bands description

No	Indices	Full name	Formula Based on S2 bands
1	NDVI	Normalised Difference Vegetation Index	$\frac{NNIR - R}{NNIR + R}$
2	MSAVI 2	Modified Soil Adjusted Vegetation Index	$\frac{2\times NNIR+1-\sqrt{(2\times NNIR+1)^2+8(NNIR-R)}}{2}$
3	VARI	Visible Atmospherically Resistant Index	$\frac{G - R}{G + R - B}$
4	MNDWI	Modified Normalized Difference Water Index	$\frac{G - S1}{G + S1}$
5	NDMI	Normalized Difference	$\frac{NNIR - S1}{NNIR + S1}$
6	BAI	Burn Area Index	$\frac{1}{(0.1-R)^2+(0.06-NNIR)^2}$
7	NDBI	Normalized Difference Built-up Index	$\frac{S1 - NNIR}{S1 + NNIR}$
8	EVI	Enhanced Vegetation Index	$2.5 \times \frac{NNIR-R}{NNIR+(6\times R-7.2\times B)+1}$
9	EVI2	Enhanced Vegetation Index	$2.5 \times \frac{NNIR - R}{NNIR + 2.4 \times R + 1}$
10	OSAVI	Optimised Soil Adjusted Vegetation Index	$\frac{NNIR - R}{NNIR + R + 0.16}$
11	SATVI	Soil Adjusted Total Vegetation Index	$\frac{S1 - R}{S1 + R + L} \times (1 + L) + \frac{S2}{2}$
12	BSI	Bare Soil Index	$\frac{R + B - G}{R + B + G}$
13	NDWI	Normalized Difference Water Index	$\frac{NNIR - S1}{NNIR + S1}$
14	SIPI	Structure Insensitive Pigment Index	$\frac{NNIR - CO}{NNIR + R}$
15	MSI	Moisture Stress Index	$\frac{S1}{NNIR}$
16	GNDVI	Green Normalized Difference Vegetation Index	$\frac{NNIR - G}{NNIR + G}$
17	BI	Bare Soil Index	$\frac{(S1 + R) - (NNIR + B)}{(S1 + R) + (NNIR + B)}$
18	DBSI	Dry Bare Soil Index	$\frac{S1 - G}{S1 + G} - NDVI$
19	NBAI	Normalised Built-Up Area Index	$\frac{S2 - S1/G}{S2 + S1/G}$
20	BRBA	Band Ratio for Built-Up Area	$\frac{R}{S1}$

No	Indices	Full name	Formula Based on S2 bands
21	GI	Greenness Index	$\frac{G}{R}$
22	MSR	Modified Simple Ratio	$\frac{SR - 1}{\sqrt{SR - 1}}$
23	SR	Simple Ratio	$NNIR/R$
24	RDVI	Renormalised Difference Vegetation Index	$\frac{NNIR - R}{\sqrt{NNIR + R}}$
25	NRI	Nitrogen Reflectance Index	$\frac{G - R}{G + R}$
26	TCARI	Transformed Chlorophyll Absorption and Reflectance Index	$3\left[(RE1 - R) - 0.2(RE1 - G)\left(\frac{RE1}{R}\right)\right]$
27	PSRI	Plant Senescence Reflectance	$\frac{R - B}{RE2}$
28	NPCI	Normalised Pigment Chlorophyll ratio Index	$\frac{R - Co}{R + Co}$
29	MCARI _alt	Modified Chlorophyll Absorption in Reflectance Index (alternate)	$((RE1 - R) - 0.2 \times (RE1 - G) * (\frac{RE1}{R}))$
30	MTCI	Merris Terrestrial Chlorophyll Index	$\frac{(NNIR - RE2)}{(RE2 + R)}$
31	MCARI	Modified Chlorophyll Absorption in Reflectance Index	$\frac{[(NNIR - RE1) - 0.2(NNIR - G)]}{RE1}$
32	CCCI_alt	Canopy Chlorophyll Content (alternate)	$\frac{\left(\frac{NNIR - RE2}{NNIR + RE2}\right)}{\left(\frac{NNIR - R}{NNIR + R}\right)}$
33	CVI	Chlorophyll Vegetation Index	$NNIR \times \frac{R}{G^2}$
34	AVI	Advanced Vegetation Index	$\sqrt[3]{(NNIR \times (1 - R)) \times (NNIR - R)}$
35	PVR	Photosynthetic Vigour Ratio	$\frac{G - R}{G + R}$
36	IRECI	Inverted Red Edge Chlorophyll Index	$\frac{\rho \times NNIR - \rho \times R}{\frac{\rho\times RE2}{\rho\times RE1}}$
37	ARVI2	Atmospherically Resistant Vegetation Index 2	$-0.18 + 0.17\left(\frac{NNIR - R}{NNIR + R}\right)$
38	mNDVI	Modified NDVI	$\frac{(NNIR - R)}{NNIR - R + 2 \times CO}$

https://doi.org/10.5194/isprs-archives-XLVIII-M-1-2023-73-2023 | © Author(s) 2023. CC BY 4.0 License.

No	Indices	Full name	Formula Based on S2 bands
39	MNDRE	Modified Normalised Difference Red-edge	$\frac{(RE2-RE1)}{RE2-RE1+2\times CO}$
40	MACC	Maccioni	$\frac{(RE3-RE1)}{RE3+R}$
41	Datt	Datt	$\frac{(NNIR-RE1)}{(NNIR+R)}$
42	NDVI2	NDVI2	$\frac{(RE2-RE1)}{(RE2+RE1)}$
43	NDVI3	NDVI3	$\frac{(R-G)}{(R+G)}$
44	MTCI_at	Meris Terrestrial Chlorophyll Index	$\frac{(RE2-RE1)}{RE1-R}$
45	BUI	Built-up Index	$\left(\frac{S1-NNIR}{S1+NNIR}\right)-\left(\frac{NNIR-R}{NNIR+R}\right)$
46	NDWI_G_N	Normalised Difference Water Index (using G and N bands)	$\frac{G-NNIR}{G+NNIR}$
47	NMDI	Normalised Multiband Drought Index	$\frac{(NNIR-(S1-S2))}{(NNIR+(S1-S2))}$
48	NDRE	Normalised Difference Red Edge	$\frac{NNIR-RE1}{NNIR+RE1}$
49	CCCI	Canopy Content Chlorophyll Index	$\frac{(NNIR-RE2)/(NNIR+RE2)}{(NNIR-R)/(NNIR+R)}$
50	SELI	Sentinel Estimated Leaf-Area Index	$\frac{NNIR-RE1}{NNIR+RE1}$
51	LAI_alt	Leaf-Area Index (alternate)	SELI*5.405-0.114
52	DM_NDVI	Dry Mass using NDVI	NDVI*12.3245-5.70

Table 4. Index description

https://doi.org/10.5194/isprs-archives-XLVIII-M-1-2023-73-2023 | © Author(s) 2023. CC BY 4.0 License.